Induced versus intrinsic magnetic moments in ultrafast magnetization dynamics

M. Hofherr,[1,2,*] S. Moretti,[3] J. Shim,[4,5] S. Häuser,[1] N. Y. Safonova,[6] M. Stiehl,[1] A. Ali,[4,5] S. Sakshath,[1] J. W. Kim,[5,7]
D. H. Kim,[8] H. J. Kim,[9] J. I. Hong,[9] H. C. Kapteyn,[10] M. M. Murnane,[10] M. Cinchetti,[11] D. Steil,[12] S. Mathias,[12]
B. Stadtmüller,[1,2] M. Albrecht,[6] D. E. Kim,[4,5] U. Nowak,[3] and M. Aeschlimann[1]

[1]*Department of Physics and Research Center OPTIMAS, Technische Universität Kaiserslautern,
Erwin-Schroedinger Strasse 46, 67663 Kaiserslautern, Germany*
[2]*Graduate School Materials Science in Mainz, Staudinger Weg 9, 55128 Mainz, Germany*
[3]*Universität Konstanz, Universitätsstraße 10, 78464 Konstanz, Germany*
[4]*Department of Physics & Center for Attosecond Science and Technology, POSTECH, Pohang 37673, South Korea*
[5]*Max Planck POSTECH/KOREA Research Initiative, Pohang 37673, South Korea*
[6]*Institute of Physics, University of Augsburg, Universitätsstraße 1, 86135 Augsburg, Germany*
[7]*Department of Physics, Kunsan National University, Kunsan 54150, South Korea*
[8]*Department of Physics, Chungbuk National University, Cheongju 28644, South Korea*
[9]*Department of Emerging Materials Science, DGIST, Daegu 42988, South Korea*
[10]*Department of Physics and JILA, University of Colorado and NIST, Boulder, Colorado 80309, USA*
[11]*Experimentelle Physik VI, Technische Universität Dortmund, 44221 Dortmund, Germany*
[12]*Georg-August-Universität Göttingen, I. Physikalisches Institut, Friedrich-Hund-Platz 1, 37077 Göttingen, Germany*

Ferromagnetic metal alloys are today commonly used in spintronic and magnetic data storage devices. These multicompound structures consist of several magnetic sublattices exhibiting both intrinsic and induced magnetic moments. Here, we study the response of the element-specific magnetization dynamics for thin film systems based on purely intrinsic (CoFeB) and partially induced (FePt) magnetic moments using extreme ultraviolet pulses from high-harmonic generation (HHG) as an element-sensitive probe. In FePt, on the one hand, we observe an identical normalized transient magnetization for Fe and Pt throughout both the ultrafast demagnetization and the subsequent remagnetization. On the other hand, Co and Fe show a clear difference in the asymptotic limit of the remagnetization process in CoFeB, which is supported by calculations for the temperature-dependent behavior of the equilibrium magnetization using a dynamic spin model. Thus, in this work, we provide a vital step toward a comprehensive understanding of ultrafast light-induced magnetization dynamics in ferromagnetic alloys with sublattices of intrinsic and induced magnetic moments.

I. INTRODUCTION

Ferromagnetic alloys are important constituents of current magnetic and spintronic devices. Our understanding of the thermal magnetic properties of these alloys often rests upon the assumption that thermal excitations can be understood in terms of a Heisenberg-type model, where the atomic magnetic moments are considered rigid in magnitude, and therefore thermal excitation appears in the form of magnons. The assumption that magnetic moments are constant in magnitude is often a good approximation [1], in particular for elemental ferromagnets. The situation is far more complex for ferromagnetic alloys where magnetic moments are located on different (elemental) sublattices. In many cases, the magnetic moments of the individual sublattices are intrinsic properties of the corresponding atoms of the specific alloy. However, in other cases, the magnetic moments of at least one of the elemental constituents are induced by the exchange field of the surrounding atoms [2–7]; i.e., the magnitude and orientation

of induced magnetic moments is determined by the other sublattices.

To design future materials for ultrafast spintronic applications, it is therefore crucial to investigate how the nature of the atomic magnetic moments (intrinsic versus induced) influences the ultrafast magnetization dynamics in magnetic alloy structures. To date, only a few element-specific studies of ferromagnetic (such as NiPd [8], CoPd [9], and FeNi [9,10]) and ferrimagnetic alloys (such as FeGd [11] and DyCo$_5$ [9]) have been reported. While these investigations revealed surprisingly strong sublattice-specific magnetization dynamics, they only focused on alloys with intrinsic magnetic moments on both sublattices. This naturally raises the intriguing question if a similar sublattice-specific behavior can also be observed for ferromagnetic alloys with induced magnetic moments on one sublattice. The main reason for the limited experimental studies reported thus far is the significant experimental challenge of measuring element-specific magnetic dynamics on femtosecond timescales.

One solution for addressing this challenge is to use photon energies that are resonant with distinct atomic absorption edges as a probe, which provide enhanced element-sensitive

*m.hofherr@physik.uni-kl.de

magnetic contrast. Most commonly, photon energies at the *L*-absorption edges of the magnetic materials (available at synchrotron light sources or free electron laser facilities) can be used to perform x-ray magnetic circular dichroism (XMCD) and x-ray diffraction experiments [12–14]. More recently, photons in the extreme UV region generated by high-harmonic generation (HHG) can enable ultrafast transversal magneto-optical Kerr effect (TMOKE) or circular dichroism [10,15–18] measurements at the *M*-absorption edges.

In this work, we utilize the HHG-TMOKE approach to investigate the technologically important ferromagnetic alloys CoFeB [19–22] and FePt [3,4,23–26]. These materials represent model systems with either purely intrinsic magnetic moments on the magnetic sublattices (Co and Fe sites of CoFeB) or with induced magnetic moments on one magnetic sublattice (Pt site of FePt). We investigate both the demagnetization as well as the remagnetization process for both systems. Most interestingly, we observe a distinct, element-specific remagnetization behavior for the CoFeB alloy, whereas no such behavior is found for the magnetic moments in FePt. We connect this behavior to the temperature dependence of the equilibrium magnetization obtained via an atomistic spin model, which strongly suggests a thermal origin for this effect.

II. EXPERIMENTAL DETAILS: SAMPLE SYSTEMS AND EXPERIMENTAL SETUP

We investigated two CoFeB samples ($Co_{60}Fe_{20}B_{20}$) with a film thickness of 5 nm deposited by magnetron sputtering at room temperature on two different insulating oxide surfaces with different thermal conductivity: SiO_2 and $CoNiO/SiO_2$. Both samples were capped with a 2-nm-thick Ta layer to prevent oxidation. As CoNiO is an antiferromagnetic material, we do not observe a magnetic signal in HHG-TMOKE from this layer. The 5-nm-thick FePt sample was also prepared by magnetron sputtering at room temperature on an oxidized Si(100) substrate without using a capping layer. The FePt film is polycrystalline and exhibits the chemically disordered fcc structure (*A*1 phase).

In our pump-probe experiments, we used an infrared pump beam with a central wavelength of 780 nm, a repetition rate of 6 kHz, and a full width at half maximum (FWHM) of ∼30 fs to optically excite the electronic system of our samples. For both CoFeB samples, we used a laser fluence of 5.0 mJ/cm² to obtain a magnetization quenching of ∼25%. This value was determined at the sample position and hence only reflects the photon density irradiated onto the sample surface. For FePt, about the same quenching is achieved for a fluence of 0.6 mJ/cm² indicating a similar amount of absorbed energy in the material. The different fluence required for the same reduction of magnetization of FePt and CoFeB is most likely due to a different reflectivity of both samples and the much higher spin-flip scattering rate of FePt compared to CoFeB leading to a much more efficient demagnetization process of FePt compared to CoFeB [16,27,28]. To probe the magnetization dynamics, we employ extreme ultraviolet (XUV) light in the range of 30–70 eV generated by HHG in a neon-filled hollow waveguide [29,30].

To extract magnetic information in the experiment, we measure the spectrally resolved reflected intensities I_+ and I_-

with two opposing external magnetic fields being applied alternately. Subsequently, we calculate the magnetic asymmetry by $A = \frac{I_+ - I_-}{I_+ + I_-}$ as depicted for CoFeB in Fig. 1(a). Notably, the magnetic asymmetry is resonantly enhanced close to the $M_{2,3}$-absorption edges (Fe: ∼52 eV; Co: ∼59 eV) enabling us to simultaneously probe the magnetic responses assigned to both elements.

III. EXPERIMENTAL RESULTS

We first consider the optically induced magnetization dynamics for CoFeB/CoNiO as a typical model system for a ferromagnetic alloy with intrinsic magnetic moments on both Co and Fe sites. The corresponding magnetization traces on a timescale of 1 and 140 ps are shown in Figs. 1(b) and 1(c), respectively. They were obtained by numerical integration of the asymmetry in the colored shaded energy regions in Fig. 1(a). These energy regions were chosen to minimize the overlap between the absorption edge signals of the Fe and Co sublattice which was determined to be smaller than 2%.

Right after the optical excitation, both magnetic sublattices demagnetize almost simultaneously and we observe a slight deviation of the transient magnetization dynamics of Fe and Co which is still within our experimental uncertainty. Small differences in the ultrafast magnetization dynamics right after the optical excitation have already been reported previously. For a Ni-Fe alloy with intrinsic magnetic moments on both sublattices, past work observed a ≈20–80-fs time lag between Fe and Ni in a pure and Cu-diluted FeNi ferromagnetic alloy [10]. The remagnetization process of CoFeB starts approximately after 500 fs, i.e., after the maximum level of demagnetization was reached. Interestingly, we observe clearly a different asymptotic behavior in the remagnetization process for Fe and Co as shown in Fig. 1(c).

A qualitative explanation of the different regimes passing through during the de- and remagnetization process can be derived from the microscopic three-temperature model [(M3TM) see Fig. 1(d)] [31], which describes the exchange of energy and angular momentum between the subsystems of electrons, spins, and lattice: Throughout the demagnetization the spin system is efficiently heated during the first few hundred femtoseconds by energy transfer from the electron system (regime I). Subsequently, the electron, spin, and phonon systems equilibrate within 0.5–5 ps resulting in a cooling process and consequently in a magnetization increase (regime II). On longer timescales this cooling process of all systems continues via a slow heat exchange with the environment, for instance, with a substrate or buffer layer (regime III). A comparison with a measurement of CoFeB deposited directly on the insulating SiO_2 substrate with comparable quenching [see Fig. 2(a)] reveals very similar dynamics: Within the larger error bars, the demagnetization is again overlapping while the asymptotic limit in the remagnetization for Co and Fe differs. Notably, the normalized asymptotic values are smaller for CoFeB/SiO_2 compared to CoFeB/CoNiO/SiO_2 suggesting a dependence of this dynamics on the thermal conductivity of the film underneath the CoFeB. This is expected to be quite different for these two samples, as will be discussed later.

We now turn to FePt on SiO_2. Here, the magnetic moments on the Pt sites are induced by the exchange field of the
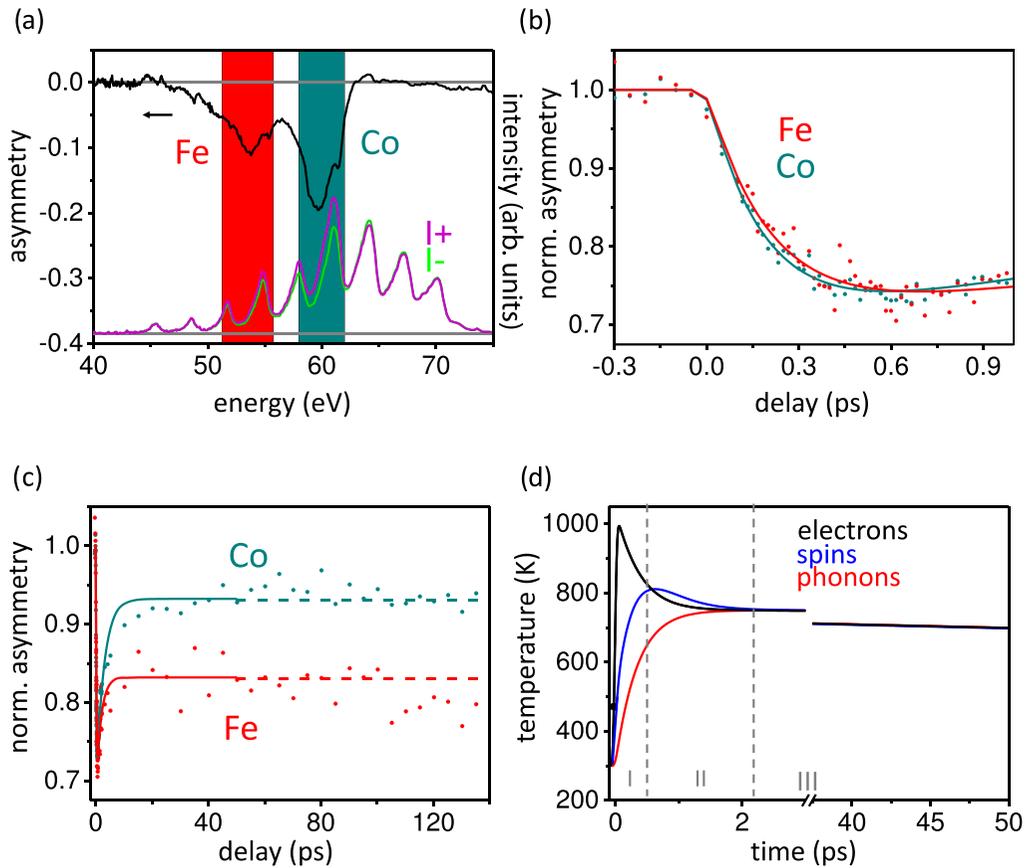
FIG. 1. (a) Reflected intensity for two opposite magnetization directions (green and purple lines) and corresponding magnetic asymmetry of CoFeB/CoNiO/SiO$_2$ (black line). The shaded areas are integrated for each time delay to create the dynamical traces. (b,c) Ultrafast demagnetization and remagnetization dynamics of Co and Fe. The straight lines are exponential guides to the eye. After initially demagnetizing with the same rate and amplitude (b) the remagnetization in Co is much stronger (c). This is due to a stronger exchange field of Co leading to a higher relative magnetization at the same temperature. (d) Typical three-temperature calculation for Fe revealing three different timescales during the demagnetization: (I) Heating of the spin system by the electrons, (II) equilibration between electron spins and phonons, and (III) heat exchange with the environment (e.g., the substrate).

intrinsic moments on the surrounding Fe sites [3,4,32–34]. The static asymmetry of FePt on SiO$_2$ is shown in Fig. 2(b), the corresponding element-specific demagnetization and relaxation dynamics for a similar maximum quenching as for the CoFeB samples in Figs. 2(c) and 2(d). On short timescales right after the optical excitation, we again observe an identical magnetization dynamics for Fe and Pt, in accordance to our findings for CoFeB. In addition, this behavior also agrees with the ultrafast element-specific magnetization dynamics of a Pt/Co/Pt multilayer film [16] for which the magnetic moments of the Pt layers are induced by the Co layer. Crucially, the element-resolved data reveal equal de- and remagnetization amplitudes for Fe and Pt, in contrast to the CoFeB case with intrinsic magnetic moments. The magnetization dynamics of the induced Pt moments hence follows the dynamics of the Fe sites throughout the measurement.

IV. LOCALIZED SPIN MODEL SIMULATIONS AND DISCUSSION

In the following section, we will discuss our results within the framework of a localized spin model. We focus on the

most interesting difference in the spin dynamics of FePt and CoFeB, namely, the distinct, element-specific remagnetization behavior for the magnetic heterostructure CoFeB/CoNiO which was not observed for FePt. The magnetization of the Pt sublattice is always proportional to that of the Fe sublattice.

The explanation for the equal de- and remagnetization amplitudes for FePt is straightforward: Since the magnetic moment in Pt is induced by the exchange field of the surrounding Fe atoms [4], the Pt magnetization naturally follows the magnetization of the Fe sublattice. Mryasov *et al.* [4] calculated the exchange field of a fully polarized Fe sublattice acting on a Pt moment from *ab initio* methods as 27.3 meV. While the Pt-Pt exchange is practically zero, the induced Pt moment turned out to be proportional to the Fe-Pt exchange field. The calculated energy scale corresponds to a timescale of about 240 fs, where distinct dynamics could occur. Below this timescale, we cannot exclude distinct dynamics of the Fe and Pt sublattices hidden in the experimental uncertainty of our data.

The explanation for the unequal asymptotic remagnetization amplitude (Co (93±1)% and Fe (84±1)% for
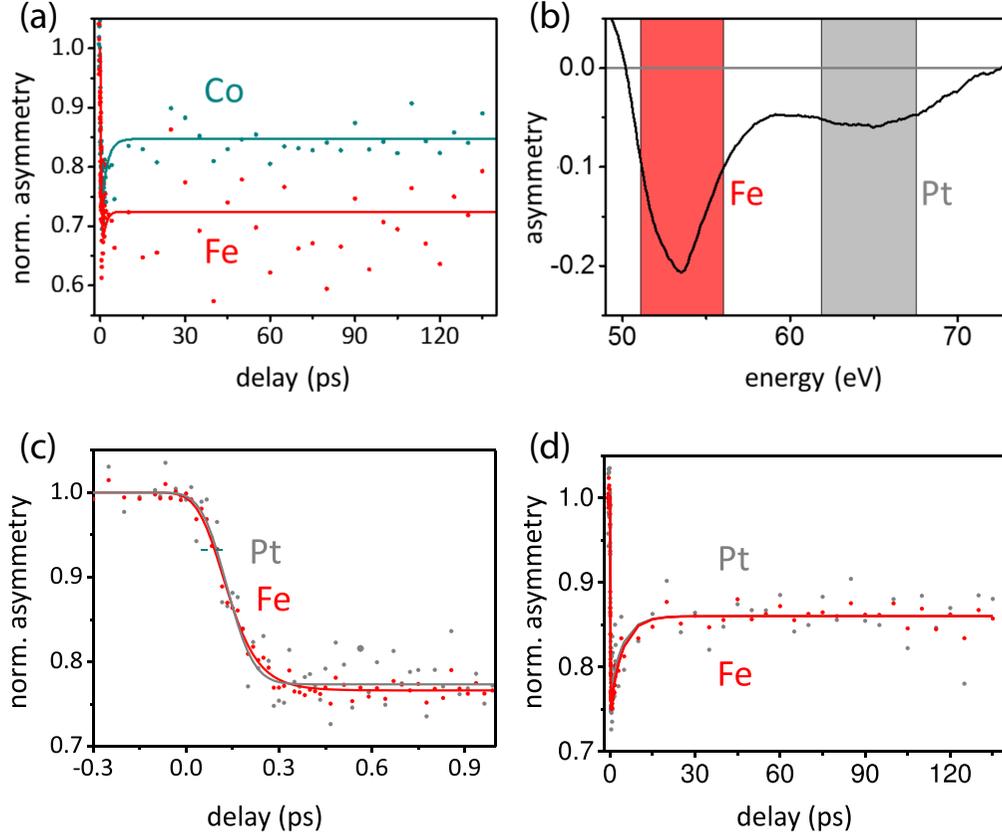
FIG. 2. (a) Ultrafast demagnetization and relaxation of CoFeB/SiO$_2$. Compared to the case of CoFeB/CoNiO/SiO$_2$ [see Fig. 1(c)] the remagnetization amplitude is smaller. Panel (b) shows the static asymmetry of the FePt sample with clearly distinguishable Fe and Pt signals. Panels (c,d) illustrate the transient demagnetization and remagnetization traces of FePt/SiO$_2$ on a 1-ps (c) and 140-ps (d) timescale. The induced moment of Pt follows the behavior of Fe in contrast to the reaction of the intrinsic moments in CoFeB (a).

CoFeB/CoNiO) for the systems with intrinsic moments on all sublattices is more challenging. The different remagnetization amplitudes seem to suggest that the spin systems of Co and Fe are not in equilibrium during the recovery process, associated with more efficient cooling of the Co system. This indicates either a different electron-phonon coupling or a different spin-flip probability on the Co and Fe sites. However, the relaxation process for both sublattices slows down rapidly after ∼20 ps suggesting a *global* equilibrium of all spins, electrons, and phonons. In particular, this also implies that the spin systems are already equilibrated. Therefore, the different asymptotic behavior directly points to a different temperature behavior of the equilibrium magnetization for the two constituents of the alloy. Indeed, this was already theoretically predicted for the case of Ni and Fe in permalloy by Hinzke *et al.* [1].

Accordingly, we performed calculations for Co and Fe using atomistic spin model simulations [1,35]. We have carried out simulations for an fcc lattice with 60% Co, 20% Fe, and 20% B atoms placed randomly on the lattice sites. We consider classical spins $S_i^\epsilon = \mu_i^\epsilon / \mu_i^\epsilon$, where μ_i^ϵ represents the magnetic moment of either Co ($\mu_i^{Co} = 1.75\ \mu_B$) or Fe ($\mu_i^{Fe} = 2.6\ \mu_B$) [36], depending on the lattice site. B atoms are represented by null spins on the lattice ($S_i^B = 0$). The spin

Hamiltonian for the unitary vectors S_i^ϵ is given by

$$\mathcal{H} = -\sum_{ij} \left[\frac{\mathcal{J}_{ij}}{2} S_i^\epsilon \cdot S_j^\delta - \left(\frac{\mu_0 \mu_i^\epsilon \mu_j^\delta}{8\pi} \right) \right. $$
$$\left. \times \frac{3(S_i^\epsilon \cdot \mathbf{e}_{ij})(\mathbf{e}_{ij} \cdot S_j^\delta) - S_i^\epsilon \cdot S_j^\delta}{r_{ij}^3} \right], \quad (1)$$

where the first term represents the exchange interaction and the second term indicates the dipolar interaction. μ_0 is the vacuum permeability and r_{ij} is the distance between spins. $\mathcal{J}_{ij}$ represents the exchange interaction matrix, which we consider different from zero only for nearest neighbors. Note that $\mathcal{J}_{ij} = \mathcal{J}_{Fe\text{-}Fe}$, $\mathcal{J}_{Co\text{-}Co}$, or $\mathcal{J}_{Fe\text{-}Co}$, depending on the kind of neighbor. In particular, we used $\mathcal{J}_{Fe\text{-}Fe}^0 = 5.05$ mRy [36], $\mathcal{J}_{Co\text{-}Co}^0 = 15.63$ mRy [37], and $\mathcal{J}_{Fe\text{-}Co}^0 = 7.01$ mRy. This latter value is obtained by fitting with the experimental data. The lattice constant is set to $a = 0.368$ nm, as used in the calculation of the exchange integrals of fcc Fe [36].

Within this choice of the exchange integrals, we obtained a Curie temperature of $T_C \sim 700$ K, in agreement with experimental results for similar, not-annealed CoFeB samples [38].

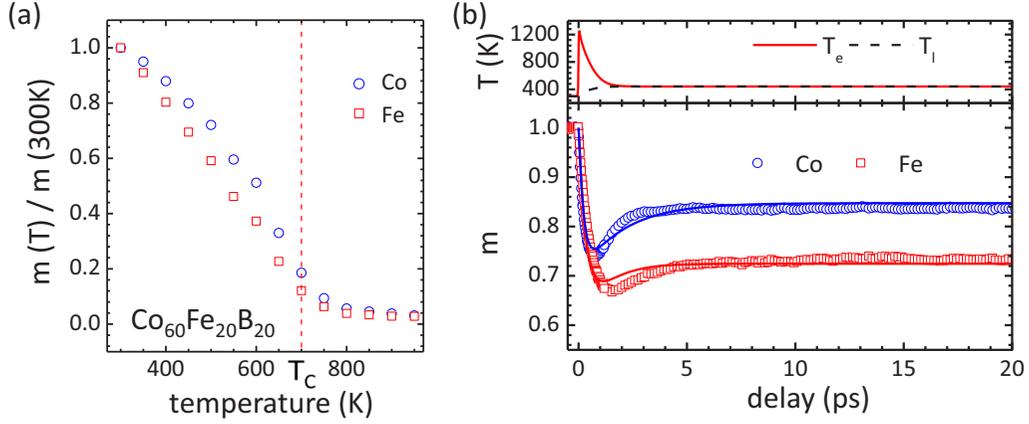The temporal evolution of the spin system is obtained by solving the stochastic Landau-Lifshitz-Gilbert (LLG)

FIG. 3. (a) Normalized element-specific zero-field equilibrium magnetization of either Co and Fe as a function of temperature calculated by atomistic spin dynamics. For all temperatures Co has a higher relative magnetization than Fe matching the experimental results. For comparison, the calculated saturation magnetization of Co is 781 kA/m, the one of Fe 387 kA/m. (b) Simulations of the de- and remagnetization of Co and Fe compared to the guidelines of Fig. 2(a). The transition from a uniform demagnetization to an independent remagnetization is well reproduced.

equation for each spin:

$$\frac{dS_i^\epsilon}{dt} = -\frac{\gamma_\epsilon}{(1 + \lambda_\epsilon^2)\mu^\epsilon} S_i \times [H_i + \lambda_\epsilon(S_i \times H_i)], \quad (2)$$

where γ_ϵ and λ_ϵ represent the gyromagnetic ratio and the damping parameters of the two sublattices, respectively. The effective field H_i is given by $H_i = -\frac{\partial \mathcal{H}}{\partial S_i^\epsilon} + \zeta_i(t)$, where ζ_i represents a stochastic field with the following properties:

$$\langle \zeta_i(t) \rangle = 0, \quad \langle \zeta_{i\eta}(0)\zeta_{j\theta}(t) \rangle = \frac{2k_B T_e \lambda_\epsilon \mu_\epsilon}{\gamma_\epsilon} \delta_{ij}\delta_{\eta\theta}\delta(t), \quad (3)$$

where k_B is the Boltzmann constant and T_e is the electron temperature. Here, i, j denote lattice sites while η, θ denote Cartesian components. Details about the algorithms used to solve Eq. (2) are described in Ref. [35].

The dynamics of the electron and phonon temperatures is calculated by means of a two-temperature model [39,40], described by Eqs. (4) and (5), which allows us to separate electron (T_e) from lattice (T_l) temperatures:

$$\gamma_e T_e \frac{dT_e}{dt} = \frac{\partial}{\partial z}\left(k_e \frac{\partial T_e}{\partial z}\right) - g_{ep}(T_e - T_l) + P(t, z), \quad (4)$$

$$C_l \frac{dT_l}{dt} = g_{ep}(T_e - T_l). \quad (5)$$

$\gamma_e T_e$ and C_l represent the electron and lattice heat capacity, respectively, while g_{ep} is the electron-phonon coupling constant. $k_e = k_e^0 T_e/T_l$ is the electron thermal conductivity and $P(t, z) = \alpha A F g(t)e^{-\alpha z}$ is the absorbed power per unit volume. α is the optical penetration depth, A is the absorbed power, and F is the fluence of the laser. $g(t)$ represents a Gaussian function with FWHM = 30 fs describing the temporal profile of the laser pulse. We used thermal parameters calculated for Co [40]. The optical penetration depth for a laser wavelength of 780 nm is $\alpha^{-1} \sim 13$ nm [41]. We set the fluence to the experimental value ($F = 5$ mJ/cm^2) and we use the absorbed power A and the damping λ^ϵ as free

parameters. We consider a system of $32 \times 32 \times 32$ spins and simulate the temperature and magnetization dynamics by solving Eqs. (2), (4), and (5), simultaneously.

The results are shown in Fig. 3 for $\lambda_{Co} = \lambda_{Fe} = 0.004$ and $A = 17.5\%$. Note that the damping parameter λ is in agreement with the experimental results for bulk CoFeB [42]. Figure 3(a) represents the equilibrium magnetization of each sublattice as a function of temperature normalized to the value at $T_0 = 300$ K. Despite the common Curie temperature ($T_C \sim 700$ K), the equilibrium magnetization can be different below T_C. Figure 3(b) represents the temperature and magnetization dynamics compared to the experimental results marked by the guidelines taken from Fig. 2(a). The magnetization dynamics is obtained by averaging over five stochastic realizations. The agreement to the experimental data is remarkably good, especially if we consider the uncertainty on the exchange and thermal parameters. The general trend is indeed intuitive since Co has a stronger exchange field, leading to a stronger Co-Co interaction and a smaller disorder for low temperatures. This correlation between a stronger exchange field and a larger equilibrium magnetization was already demonstrated for bulk and surface states by Stampanoni *et al.* [43] using spin-resolved photoemission.

The explanation for the different normalized asymptotic limits during the remagnetization process is supported by our results of CoFeB deposited on SiO$_2$ and CoNiO with different thermal conductivity. For the case of CoFeB/SiO$_2$ [see Fig. 2(a)] these asymptotic values are smaller compared to the case of CoFeB/CoNiO/SiO$_2$ [Fig. 1(c)] since the thermal conductivity of SiO$_2$ is about an order of magnitude smaller than that of ferromagnet oxides [44,45], i.e., CoNiO, acting as a more efficient heat sink. Thus, for SiO$_2$, the spin, phonon, and electron systems of both Fe and Co equilibrate to a higher temperature in the observed time frame of 140 ps resulting in a smaller magnetization. Our findings hence show that the asymptotic values of the remagnetization process are determined by the different temperature dependence of the equilibrium magnetization of both magnetic sublattices in CoFeB.

V. CONCLUSION

In conclusion, we used time-resolved HHG-TMOKE to study the de- and remagnetization dynamics of magnetic constituents in ferromagnetic alloys for the cases of intrinsic and induced magnetic moments on the individual sublattices. On the one hand for FePt, the Pt moment induced by the Pt-Fe exchange lacks a direct Pt-Pt exchange interaction, and consequently, its magnetization always follows that of Fe. Therefore, their relative dynamics match during both the demagnetization and remagnetization process. In contrast, CoFeB as a representative for a ferromagnetic alloy with intrinsic magnetic moments shows approximately identical demagnetization for Co and Fe, while the normalized remagnetization amplitudes clearly differ. This behavior is caused by the different exchange constants for the Co-Co and Fe-Fe interactions, resulting in an element-specific temperature dependence of the equilibrium magnetizations of the two sublattices. Thus, even though the two respective spin systems converge toward a common equilibrium temperature during the relaxation process, the relative magnetization follows a distinct trend. Calculations using atomistic spin model simulations support this argument matching the temporal evolution for Co and Fe. We believe that these findings are of a general nature and can be extended to a variety of magnetic alloys, which can accordingly be separated into two classes, those with either induced or intrinsic magnetization dynamics. Hence, this work has a significant impact for fundamental studies on ultrafast magnetization dynamics in magnetic alloys, which are crucial for the development of faster next-generation spintronic devices.

[1] D. Hinzke, U. Atxitia, K. Carva, P. Nieves, O. Chubykalo-Fesenko, P. M. Oppeneer, and U. Nowak, Phys. Rev. B **92**, 054412 (2015).

[2] F. Menzinger and A. Paoletti, Phys. Rev. **143**, 365 (1966).

[3] O. N. Mryasov, Phase Trans. **78**, 197 (2005).

[4] O. N. Mryasov, U. Nowak, K. Y. Guslienko, and R. W. Chantrell, Europhys. Lett. **69**, 805 (2005).

[5] M. Ležaić, P. Mavropoulos, G. Bihlmayer, and S. Blügel, Phys. Rev. B **88**, 134403 (2013).

[6] J. Crangle, Philos. Mag. **5**, 335 (1960).

[7] S. J. Pickart and R. Nathans, J. Appl. Phys. **33**, 1336 (1962).

[8] S.-G. Gang, R. Adam, M. Plötzing, M. V. Witzleben, C. Weier, U. Parlak, D. E. Bürgler, C. M. Schneider, J. Rusz, P. Maldonado, and P. M. Oppeneer, Phys. Rev. B **97**, 064412 (2018).

[9] I. Radu, C. Stamm, A. Eschenlohr, F. Radu, R. Abrudan, K. Vahaplar, T. Kachel, N. Pontius, R. Mitzner, K. Holldack, A. Föhlisch, T. A. Ostler, J. H. Mentink, R. F. L. Evans, R. W. Chantrell, A. Tsukamoto, A. Itoh, A. Kirilyuk, A. V. Kimel, and T. Rasing, SPIN **05**, 1550004 (2015).

[10] S. Mathias, C. La-O-Vorakiat, P. Grychtol, P. Granitzka, E. Turgut, J. M. Shaw, R. Adam, H. T. Nembach, M. E. Siemens, S. Eich, C. M. Schneider, T. J. Silva, M. Aeschlimann, M. M. Murnane, and H. C. Kapteyn, Proc. Natl. Acad. Sci. USA **109**, 4792 (2012).

[11] I. Radu, K. Vahaplar, C. Stamm, T. Kachel, N. Pontius, H. A. Dürr, T. A. Ostler, J. Barker, R. F. L. Evans, R. W. Chantrell, A. Tsukamoto, A. Itoh, A. Kirilyuk, T. Rasing, and A. V. Kimel, Nature **472**, 205 (2011).

[12] C. Stamm, T. Kachel, N. Pontius, R. Mitzner, T. Quast, K. Holldack, S. Khan, C. Lupulescu, E. F. Aziz, M. Wietstruk, H. A. Dürr, and W. Eberhardt, Nat. Mater. **6**, 740 (2007).

[13] M. Wietstruk, A. Melnikov, C. Stamm, T. Kachel, N. Pontius, M. Sultan, C. Gahl, M. Weinelt, H. A. Dürr, and U. Bovensiepen, Phys. Rev. Lett. **106**, 127401 (2011).

[14] M. Först, R. I. Tobey, S. Wall, H. Bromberger, V. Khanna, A. L. Cavalieri, Y.-D. Chuang, W. S. Lee, R. Moore, W. F. Schlotter, J. J. Turner, O. Krupin, M. Trigo, H. Zheng, J. F. Mitchell, S. S. Dhesi, J. P. Hill, and A. Cavalleri, Phys. Rev. B **84**, 241104 (2011).

[15] C. La-O-Vorakiat, E. Turgut, C. A. Teale, H. C. Kapteyn, M. M. Murnane, S. Mathias, M. Aeschlimann, C. M. Schneider, J. M. Shaw, H. T. Nembach, and T. J. Silva, Phys. Rev. X **2**, 11005 (2012).

[16] F. Willems, C. T. L. Smeenk, N. Zhavoronkov, O. Kornilov, I. Radu, M. Schmidbauer, M. Hanke, C. von Korff Schmising, M. J. J. Vrakking, and S. Eisebitt, Phys. Rev. B **92**, 220405 (2015).

[17] T. Fan, P. Grychtol, R. Knut, C. Hernández-García, D. D. Hickstein, D. Zusin, C. Gentry, F. J. Dollar, C. A. Mancuso, C. W. Hogle, O. Kfir, D. Legut, K. Carva, J. L. Ellis, K. M. Dorney, C. Chen, O. G. Shpyrko, E. E. Fullerton, O. Cohen, P. M. Oppeneer, D. B. Milošević, A. Becker, A. A. Jaroń-Becker, T. Popmintchev, M. M. Murnane, and H. C. Kapteyn, Proc. Natl. Acad. Sci. USA **112**, 14206 (2015).

[18] C. La-O-Vorakiat, M. Siemens, M. M. Murnane, H. C. Kapteyn, S. Mathias, M. Aeschlimann, P. Grychtol, R. Adam, C. M. Schneider, J. M. Shaw, H. Nembach, and T. J. Silva, Phys. Rev. Lett. **103**, 257402 (2009).

[19] T. Ueno, J. Sinha, N. Inami, Y. Takeichi, S. Mitani, K. Ono, and M. Hayashi, Sci. Rep. **5**, 14858 (2015).

[20] D. D. Djayaprawira, K. Tsunekawa, M. Nagai, H. Maehara, S. Yamagata, N. Watanabe, S. Yuasa, Y. Suzuki, and K. Ando, Appl. Phys. Lett. **86**, 92502 (2005).

[21] S. Ikeda, K. Miura, H. Yamamoto, K. Mizunuma, H. D. Gan, M. Endo, S. Kanai, J. Hayakawa, F. Matsukura, and H. Ohno, Nat. Mater. **9**, 721 (2010).

[22] D. C. Worledge, G. Hu, D. W. Abraham, J. Z. Sun, P. L. Trouilloud, J. Nowak, S. Brown, M. C. Gaidis, E. J. O'Sullivan, and R. P. Robertazzi, Appl. Phys. Lett. **98**, 22501 (2011).

[23] Y. K. Takahashi, R. Medapalli, S. Kasai, J. Wang, K. Ishioka, S. H. Wee, O. Hellwig, K. Hono, and E. E. Fullerton, Phys. Rev. Appl. **6**, 3200904 (2016).

[24] C.-H. Lambert, S. Mangin, B. S. D. C. S. Varaprasad, Y. K. Takahashi, M. Hehn, M. Cinchetti, G. Malinowski, K. Hono, Y. Fainman, M. Aeschlimann, and E. E. Fullerton, Science **345**, 1337 (2014).

[25] S. Sun, C. B. Murray, D. Weller, L. Folks, and A. Moser, Science **287**, 1989 (2000).

[26] J.-U. Thiele, S. Maat, and E. E. Fullerton, Appl. Phys. Lett. **82**, 2859 (2003).

[27] D. Polley, M. Pancaldi, M. Hudl, P. Vavassori, S. Urazhdin, and S. Bonetti, J. Phys. D: Appl. Phys. **51**, 84001 (2018).

[28] K. C. Kuiper, T. Roth, A. J. Schellekens, O. Schmitt, B. Koopmans, M. Cinchetti, and M. Aeschlimann, Appl. Phys. Lett. **105**, 202402 (2014).

[29] A. Rundquist, C. G. Durfee, Z. Chang, C. Herne, S. Backus, M. M. Murnane, and H. C. Kapteyn, Science **280**, 1412 (1998).

[30] H. C. Kapteyn, M. M. Murnane, and I. P. Christov, Phys. Today **58**(3), 39 (2007).

[31] B. Koopmans, G. Malinowski, F. Dalla Longa, D. Steiauf, M. Fähnle, T. Roth, M. Cinchetti, and M. Aeschlimann, Nat. Mater. **9**, 259 (2010).

[32] K. Ikeda, T. Seki, G. Shibata, T. Kadono, K. Ishigami, Y. Takahashi, M. Horio, S. Sakamoto, Y. Nonaka, M. Sakamaki, K. Amemiya, N. Kawamura, M. Suzuki, K. Takanashi, and A. Fujimori, Appl. Phys. Lett. **111**, 142402 (2017).

[33] C. Antoniak, J. Lindner, M. Spasova, D. Sudfeld, M. Acet, M. Farle, K. Fauth, U. Wiedwald, H.-G. Boyen, P. Ziemann, F. Wilhelm, A. Rogalev, and S. Sun, Phys. Rev. Lett. **97**, 117201 (2006).

[34] T. Koide, T. Shidara, K. Yamaguchi, A. Fujimori, H. Fukutani, N. Nakajima, T. Sugimoto, T. Katayama, and Y. Suzuki, Phys. Rev. B **53**, 8219 (1996).

[35] U. Nowak, in *Handbook of Magnetism and Advanced Magnetic Materials*, edited by H. Kronmüller and S. S. P. Parkin (Wiley, Chichester, UK, 2007).

[36] O. N. Mryasov, V. A. Gubanov, and A. I. Liechtenstein, Phys. Rev. B **45**, 12330 (1992).

[37] S. Frota-Pessôa, R. B. Muniz, and J. Kudrnovský, Phys. Rev. B **62**, 5293 (2000).

[38] M. Yamanouchi, A. Jander, P. Dhagat, S. Ikeda, F. Matsukura, and H. Ohno, IEEE Magn. Lett. **2**, 3000304 (2011).

[39] S. I. Anisimov, B. L. Kapeliovich, and T. L. Perelman, Zh. Eksp. Teor. Fiz. **66**, 776 (1974) [Sov. Phys. JETP **39**, 375 (1974)].

[40] J. Hohlfeld, S.-S. Wellershoff, J. Güdde, U. Conrad, V. Jähnke, and E. Matthias, Chem. Phys. **251**, 237 (2000).

[41] P. Johnson and R. Christy, Phys. Rev. B **9**, 5056 (1974).

[42] X. Liu, W. Zhang, M. J. Carter, and G. Xiao, J. Appl. Phys. **110**, 33910 (2011).

[43] M. Stampanoni, A. Vaterlaus, M. Aeschlimann, and F. Meier, Phys. Rev. Lett. **59**, 2483 (1987).

[44] F. B. Lewis and N. H. Saunders, J. Phys. C: Solid State Phys. **6**, 2525 (1973).

[45] D. G. Cahill and T. H. Allen, Appl. Phys. Lett. **65**, 309 (1994).